Micro-scale modeling of contaminant effects on surface optical properties

M.G. Gartley, J.R. Schott, and S.D. Brown
Digital Imaging and Remote Sensing Laboratory
Chester F. Carlson Center for Imaging Science
Rochester Institute of Technology
54 Lomb Memorial Drive
Rochester, NY 14623-5604

ABSTRACT

The optical properties of a surface may change significantly in response to contaminants from the environment and/or human activity. We utilize a first principles, physics-based radiometric ray tracing software package to evaluate the spectral polarimetric bi-directional reflectance distribution function (BRDF) of the virgin and contaminated surfaces. In the absence of contaminants, we find the simulated reflectance properties of randomly rough Gaussian surfaces to be well represented by micro-facet based polarimetric BRDF models. However the addition of contaminants introduces phenomenology that falls outside the basic assumptions of the micro-facet BRDF models. We will present results of BRDF simulations of painted surfaces with liquid and solid contaminants.

Keywords: Spectral, polarization, remote sensing, image simulation, scene simulation, BRDF, contaminants

1. INTRODUCTION

Hyperspectral imaging has demonstrated utility for locating targets within a complex background that are difficult to locate by traditional broadband panchromatic and infrared imaging techniques. A key requirement for many detection algorithms is knowledge of the target's spectral reflectance properties. In many cases, one simply uses the hemispherical reflectance of the target and searches the scene assuming the target is Lambertian. However, other target detection techniques may take advantage of knowing the actual bidirectional reflectance distribution function properties of the target, coupled with the source and view geometries, to more accurately find them. What's more, adding the dimension of polarization to the spectral sensing techniques may provide an even better discriminator. However, oftentimes the surface state of the target of interest is not pristine. In fact it may be dirty, weathered, or wet affecting the surface reflectance properties and the detection algorithm's ability to locate them.

Approaches to modeling the polarized BRDF (pBRDF) Mueller matrix have evolved over the years, starting most notably with a classic paper[1] by Torrance and Sparrow treating in-plane surface scattering as happening from a statistical slope distribution of mirror-like microfacets making up the surfaces' topography. Variants on this idea, such as the Beard-Maxwell[2] and Priest-Meier[3] microfacet models, are commonly used and demonstrated success for accurately capturing the phenomenology of measured pBRDF data. This being said, predicting a pBRDF for a new material based purely on knowledge of optical constants and surface texture is typically not feasible based on the limitations of the pBRDF model, lack of appropriate optical constants, and lack of precise surface geometry knowledge. In addition, pBRDF models are typically configured to support modeling of a single homogeneous surface material. For cases of non-standard surface geometries and/or in the presence of surface contaminants, an alternative approach to predicting pBRDF is warranted.

2. BACKGROUND

The section presents a brief overview of spectral reflectance and bi-directional reflectance distribution function (BRDF) concepts relevant to this research.

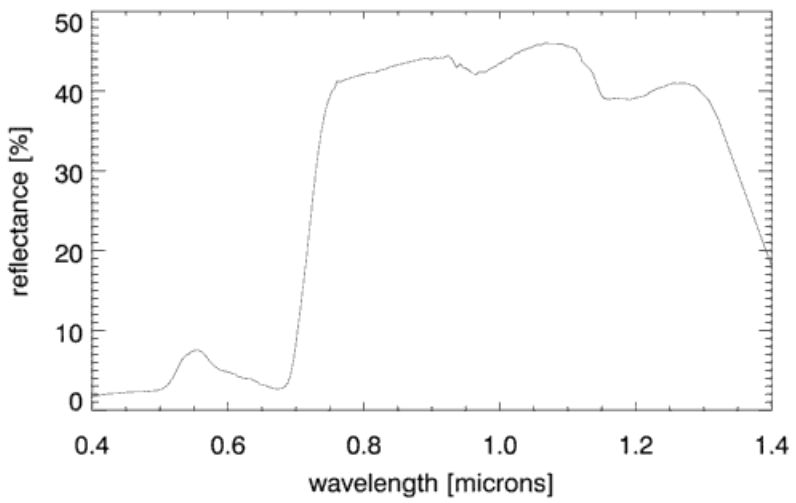

Figure 1. Spectral reflectance curve for grass measured at the Rochester Institute for Technology.

2.1 Spectral Reflectance

The spectral reflectance of a material is typically plotted as a percentage (or fraction of total incident power) versus wavelength. An example of a spectral reflectance curve for grass is presented in Figure 1. This curve typically corresponds to the total amount of incident power reflected into the hemisphere above the surface, also known as directional hemispherical reflectance (DHR),

$$DHR = \frac{M_{out}}{E_{in}} \tag{1}$$

where M_{out} is the radiant exitance and E_{in} is the irradiance incident on the surface.

2.2 Bidirectional Reflectance Distribution Function

In many remote sensing applications, one wishes to know the amount of energy that is reflected into a particular direction assuming the incident energy is coming from another particular direction. The quantity that describes this material behavior is known as the bi-directional reflectance distribution function (BRDF). This quantity is simply the ratio of the reflected radiance to the incident irradiance and has units of 1/sr.

$$\rho\left(\theta_i, \phi_i, \theta_r, \phi_r, \lambda\right) = \frac{L_{out}}{E_{in}} \tag{2}$$

It is common for most naturally occurring materials and some man-made materials to be treated as Lambertian reflectors, meaning that their BRDF value is treated as a constant independent of the incident and reflected angles. The directional hemispherical reflectance can be obtained by integrating the BRDF over the entire hemisphere above the material surface

$$DHR\left(\theta_i, \phi_i, \lambda\right) = \int \rho\left(\theta_i, \phi_i, \theta_r, \phi_r, \lambda\right) \cos\theta_i d\Omega \tag{3}$$

However, there are many materials which exhibit non-Lambertian reflectance behavior. Many man-made materials appear glossy and exhibit a strong reflectance value in the specular direction (view direction has the same zenith as the incident angle, but are rotated 180 degrees apart in azimuth). Many naturally occuring materials (such as grass and soil) exhibit a strong reflectance value in the backscattering geometry (view direction has the same zenith and azimuth as the incident direction). These cases require a non-constant BRDF value to accurately predict how the materials will appear in a remotely sensed scene.

Within the computer graphics community, there are a variety of analytical BRDF models utilized such as the Phong,[4] Cook-Torrance,[5] and Ward[6] models. The Phong and Ward models are purely empirical and have little root in the physical mechanisms involved in the reflection of light. However the Cook-Torrance model is based on a micro-facet approach to modeling a surface as a triangulated network of small mirror-like Fresnel reflectors.

Within the remote sensing community, microfacet-based BRDF models are common and have been reported on extensively. We have previously reported on a generalized form of a polarized BRDF which may be configured to match the forms of many existing microfacet-based models. The generalized form of the pBRDF contains a polarized, specular term and an unpolarized diffuse scattering term.

$$\rho = \rho_s + \rho_d \tag{4}$$

and has units of steradians^{-1}.

The polarized, specular term is written in the general form

$$\rho_s = \frac{P\left(\theta, \sigma, b\right) F\left(\theta_i, \theta_r, \phi, n, \kappa\right)}{4 \cos\theta_i \cos\theta_r} S \tag{5}$$

where θ_i and θ_r, are the incident and reflected zenith and ϕ is the relative azimuth between the incident and reflected direction. S is an arbitrary function which accounts for obscuration of the viewer and shadowing of the source by other facets, P is a surface slope probability distribution function, F is the Fresnel reflection Mueller matrix for the microfacet orientation that reflects from the incident to the desired reflection direction.

The diffuse scattering term can take many forms, but commonly contains at least a Lambertian term (no angular dependence). An example is the form utilized by the Nonconvential Exploitation Factors Database v9.5 software[7]

$$\rho_d = \rho_{d1} + \frac{\rho_{d2}}{\cos\theta_i \cos\theta_r} \tag{6}$$

where ρ_{d1} and ρ_{d2} are arbitrary constants. This form of a diffuse, multiple scatter term is purely empirical, but found to fit measured material properties quite well.

Conceivably this pBRDF model can be outfitted with a material's exact surface slope probability distribution function, complex index of refraction, and shadowing function to accurately predict its pBRDF. This is sometimes realizable for dielectric materials (such as glass or silicon) that have a well characterized surface slope distribution. However, for most materials of interest to the remote sensing community, configuring the pBRDF model based purely on optical parameters of a material of interest is not an easy task. Therefore, one typically takes the approach of measuring the pBRDF in the lab and fitting the experimental measurements to a pBRDF model for compact data storage.

We propose an alternate route to predicting material reflectance properties that does not involve lab measurements, but simply utilizing an accurate geometric representation of the surface within a rigorous ray-tracing software package to simulate polarized BRDF measurements.

3. P-BRDF MEASUREMENT SIMULATION APPROACH

We have adapted the Digital Imaging and Remote Sensing Image Generation (DIRSIG) model for simulation of polarized BRDF measurements of a wide variety of materials. The DIRSIG model is a image generation tool that utilizes a complex computational radiometry sub-system to predict absolute fluxes within a 3D scene description. The model uses [1 x 4] Stokes vector and [4 x 4] Mueller matrix calculus to propagate, reflect, transmit, etc. fluxes within the simulated scene environment. When modeling signatures the mid-wave infrared (MWIR) region (3-5 microns), the daytime illumination from the Sun is proportional to the emitted radiation from ambient (approximately 300 K) materials. Furthermore, most materials have moderate reflectances (e.g. $\rho > 0.4$) in the MWIR region and, therefore, we must consider both the reflected and the self-emission contributions to the surface leaving flux. The DIRSIG radiometry engine utilizes a single expression, governing equation across all wavelength regions such that reflected and self-emitted contributions are always included unless explicitly disabled.

Due to the level of specialized modification required to achieve the pBRDF simulation capability, it is currently kept under a separate software development branch and referred to as microDIRSIG. The prefix *micro* does not refer to a specific size scale, only that we intend to model surface and scene structure at a sub-pixel level of greater than 100x. For example, when modeling a field of grass microDIRSIG handles the geometry and radiometry associated with individual blades of grass. Another example is microDIRSIG would model individual soil particles on a dirty surface, in addition to the actual 3D topography of the surface.

One of the unique features of microDIRSIG is the ability to track the state of the detector solid angle throughout the scene as it bounces between materials. Reflection from a scene facet attributed with an analytical pBRDF requires sampling of the irradiance incident on the facet from the entire hemisphere above it, weighted by the pBRDF. However, treating a facet as perfectly specular (Fresnel reflection) results in a pBRDF with a delta function shape. Under this condition, the solid angle (in units of steradians) may also change upon reflection if the surface is not perfectly flat but curved (see Figure 2).

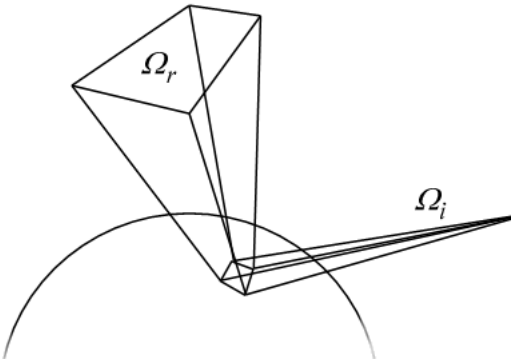

Figure 2. Schematic demonstrating the change in detector solid angle upon reflection from a curved surface.

By default, DIRSIG facets are treated as locally flat. This permits the propagation of a constant detector solid angle between specular facets. However, many surfaces are not locally flat across the span of a single detector element instantaneous field of view (IFOV), especially those containing spherical contaminant particles. microDIRSIG addresses this issue and projects not only a ray from the detector center, but also rays from all 4 corners of each detector element. The reflected detector corner rays determine the solid angle utilized to sample the hemisphere above a facet, as well as the gain/attenuation applied to incident irradiance. This feature of microDIRSIG is key to capturing specular source glints as well as maintaining the radiometric integrity of the simulation.

Another unique feature of microDIRSIG is its ability to capture a full hemispherical pBRDF measurement in one simulation run. Normally within DIRSIG, rays are cast backwards from each detector element through the scene until they reach a source of radiance (such as the sun or sky) and the radiance is cascaded back through the scene and onto the detector element. Utilizing conventional DIRSIG to simulate a BRDF measurement would result in most of the backward traced rays not hitting the source of radiance (recall that for a pBRDF measurement there is no sky!). However microDIRSIG treats each detector element as a virtual source, propogates the ray throughout the scene until it leaves the scene into the hemisphere above it and is binned into virtual detectors distributed in zenith and azimuth. The zenith angle and relative azimuth angle of each virtual detector represents a single pBRDF measurement geometry. The result is a single microDIRSIG run captures the full hemispherical pBRDF (all reflected zenith and azimuth angles) for a given incident direction.

We have previously presented[8] verification of the microDIRSIG model against analytical pBRDF models. Within statistical noise, microDIRSIG simulations match analytical pBRDF predictions very well. In fact, microDIRSIG does a more accurate job at pBRDF prediction due to the first principles nature of the simulation. microDIRSIG is not limited to single reflections, but can account for as many multiple reflections as the user desires. In addition, microDIRSIG is not limited to surface and scene textures that can only be expressed in convienient mathematical form. For example, the orientation of the surfaces of blades of grass within a field

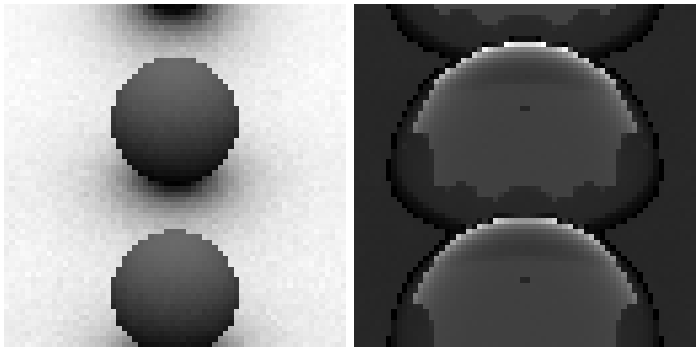

Figure 3. Visualization of two surface contaminations cases: (right) water drops on a Lambertian painted surface and (left) spherical soil particles on a moderately polarizing green painted surface.

is not easily described by a closed form mathematical function making analytical predictions on grass pBRDF difficult.

4. RESULTS

For this work, two surface contamination problems are examined (see Figure 3). The first surface is a moderately polarized, painted surface with varying levels of soil contamination on its surface. The second surface of interest is a completely unpolarized, Lambertian reflecting surface with beads of water. We chose these two examples to demonstrate the utility of microDIRSIG for predicting full spectral-polarimetric BRDFs compared to a simple linear material mixing model.

4.1 Dirty Painted Surface

The base surface material was chosen as a moderately polarized green paint. The pBRDF of the paint is well characterized and represented by a model such as the generalized model presented in Section 2. The contaminant material is soil in the form of uniformly distributed spheres across the painted surface. Alternatively, we could have chosen another fundamental geometric shape such as a cube, however we decided that spheres more accurately represented the contamination geometry of clumps of soil (future work will focus on more geometrically accurate soil representations via examination of optical microscope imagery). The soil particles are assumed to be Lambertian reflectors, with spectral reflectance values based on experimental measurements. The size of the soil particles was varied to produce contaminant area fractions between about 5 and 80%.

We chose to analyze each surface configuration at incident angles of 20 and 60 degrees. The spectral bandpass of the simulated measurement was between 0.4 and 0.9 microns with a spectral channel width of 0.05 microns. Much finer spectral resolution is available within microDIRSIG, however the channel width was kept relatively wide in order to (1) keep the simulation times reasonable and (2) the channel width was found to adequately sample the spectral features of the substrates and contaminants effectively.

Full spectral-polarimetric, hemispherical BRDFs were generated for incident angles of 20 and 60 degrees. The effective area fraction of the soil particles examined were 4.5%, 10.1%, 28.2%, 50.7%, and 77.3% under the 20 degree view angle and 9.5%, 21.3%, 54.0%, 74.5%, and 94.0% under the 60 degree view angle. Although the same particle sizes were utilized, the measured area fractions vary as a function of angle of incidence due to projected angle effects. Integrating over the entire hemisphere yields the directional hemispherical reflectance value spectrally. These results are presented in Figure 4. The microDIRSIG results are compared to results from a simple linear BRDF mixing model of the form:

$$DHR(\lambda) = f \cdot DHR_{soil}(\lambda) + (1 - f) \cdot DHR_{paint}(\lambda) \tag{7}$$

Comparison of the microDIRSIG spectral-polarimetric DHR predictions against the linear mixing model predictions shows a few interesting features. First, the microDIRSIG predictions approach the soil DHR much faster as a function of increasing soil area fraction compared to the linear mixing model predictions. Second,

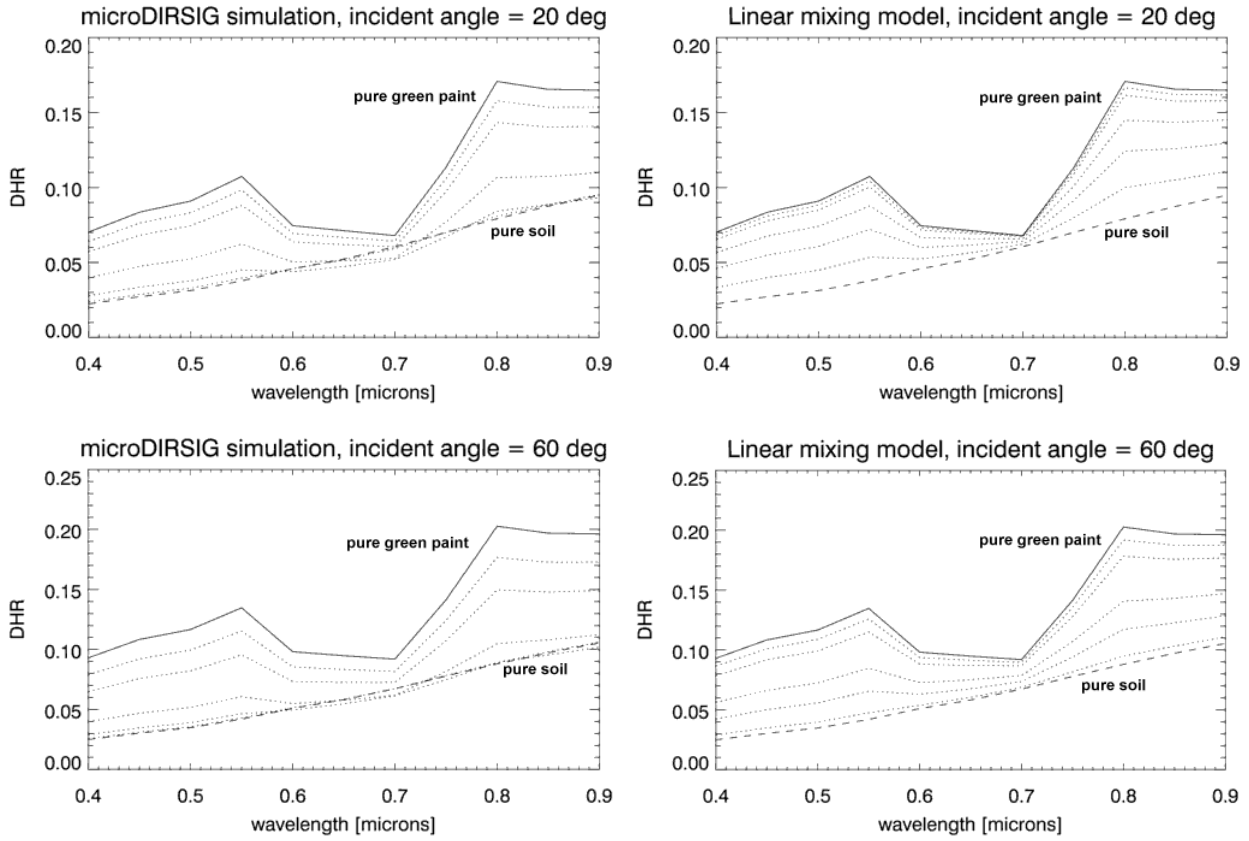

Figure 4. Spectral DHR plots of a painted surface with varying levels soil on the surface. The left column shows microDIRSIG predictions, while the right column shows predictions using a simple linear mixing reflectance model. The top row shows predictions for an incident angle of 20 degrees, and contaminant area fractions 4.5%, 10.1%, 28.2%, 50.7%, and 77.3% while the bottom row shows predictions for an incident angle of 60 degrees and contaminant area fractions 9.5%, 21.3%, 54.0%, 74.5%, and 94.0%.

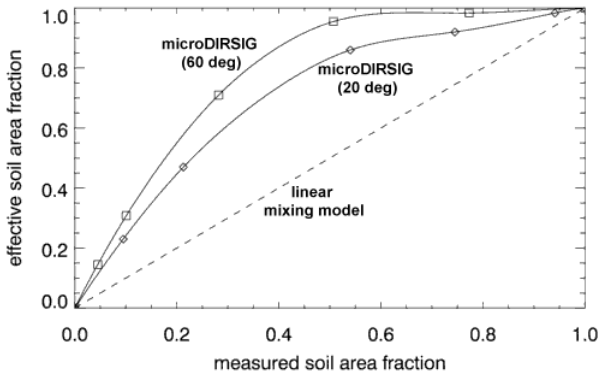

Figure 5. Relationship between measured soil area fraction versus $effective$ area fraction required for the linear mixing model to best match microDIRSIG predictions.

the spectral shape of the contaminated surfaces is not simply a spectrally constant mixture of the soil and paint DHR. In fact, the contaminated surface DHR predicted by microDIRSIG actually falls below both the soil and paint DHR at a wavelength of 0.7 microns for some soil particle area fractions. This phenomenon is believed to result from the fact that the level of diffusely reflected light is smallest for the paint at 0.7 microns (i.e. the reflected light at this wavelength is dominated by specular reflection) . The specularly reflected light is most susceptible to soil particle shadowing effects, while diffusely scattered light contributions are less effected by soil particle shadowing.

If one were to derive a non-linear mixing model from the microDIRSIG DHR predictions, the *effective* area fraction may be related to the actual measured area fraction of soil particles by a non-linear function. Figure 5 shows this relationship for incident angles of 20 and 60 degrees. This relationship is slightly more linear for the 60 degree incident angle than for the 20 degree incident angle.

Another way to examine the microDIRSIG predictions against a simple linear mixing model is to compare the derived hemispherical Degree of Polarization (DOP) of the contaminated surface (Figure 6). We may wonder, how do the soil particles attenuate the polarization signature of the painted surface? There are various ways to evaluate this. One such method involves integrating both the Stoke's S1 and S2 components over the entire hemisphere. Due to the nature of the painted surface polarization properties, the S2 component of the pBRDF integrates to 0 and the S1 component of pBRDF integrates to a positive value (indicating a net horizontal polariation) . The resulting hemispherical DOP is calculated as the ratio of the hemispherical integration of the (0,0) and (1,0) components of the pBRDF Mueller matrix.

Intuition tells us that we should expect the degree of polarization of the surface to decrease as the soil contamination increases. We indeed find this phenomenon with both the microDIRSIG and linear mixing model predictions. However the depolarization of the surface due to increasing soil contamination is is stronger in the microDIRSIG predictions compared to the linear model predictions. This is consistent with the contaminated surface DHR approaching the soil DHR, for increasing soil particle concentrations, faster within the microDIRSIG predictions due to shadowing and geometry effects not captured by the linear mixing model.

Finally, we examine the magnitude of the spectrally-integrated pBRDF as a function of scattering angle in the plane of incidence (the specular scattering plane). Examination of this plot (see Figure 7) shows the linear material mixing model does not sufficiently capture the magnitude and angular dependence of the resulting contaminated surface BRDF behavior. For example, the linear mixing model predicted specular plane BRDF has a peak in the forward scattering direction for all cases, whereas the microDIRSIG simulated BRDF has a peak that transitions from the forward scatter direction for small amounts of contamination to the backscattering direction for increasing levels of contamination. We should expect a backscattering *hotspot* due to the geometry of the soil contamination, however the linear mixing model has no knowledge of the geometry and does not capture this real effect.

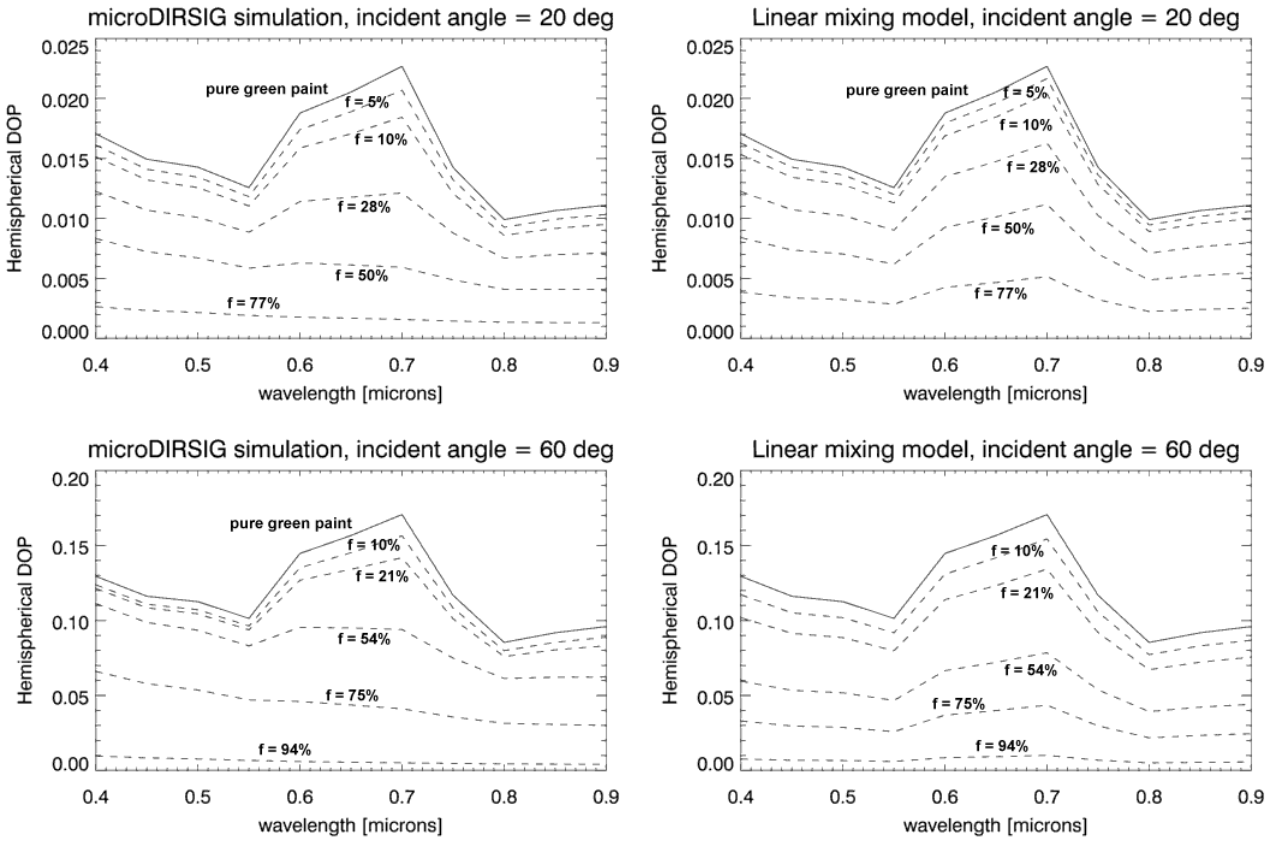

Figure 6. Spectral hemispherical degree of polarization plots of a painted surface with varying levels soil on the surface. The left column shows microDIRSIG predictions, while the right column shows predictions using a simple linear mixing reflectance model.

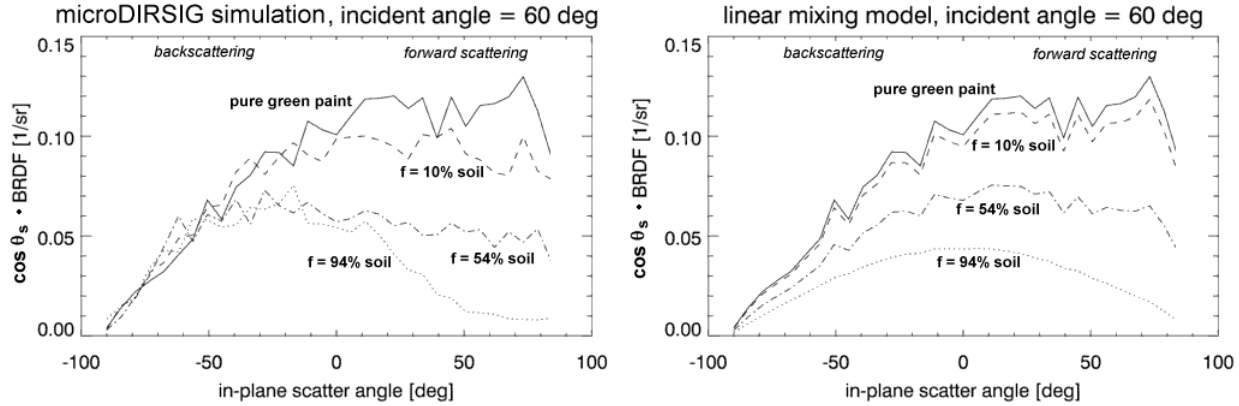

Figure 7. BRDF values in the specular scattering plane for various levels of soil contamination on a painted surface, for an angle of incidence of 60 degrees.

4.2 Wet Painted Surface

Next, we examined the case of an unpolarized, Lambertian painted surface being contaminated with water drops. The motivation was to understand how the water drops would effect the pBRDF magnitude and polarization state of reflected light from its surface.

We assumed a blacked painted surface having perfectly Lambertian scattering properties and a spectrally flat reflectance value of 4%. The contaminant in this case is water, with a spectrally dependent index of refraction. We varied both the contact angle of the water and the area fraction of the water covering the surface. The intent of this example is to examine the effect of water contact angle and area fraction on both the polarization and spectral reflectance properties of the surface. There was no significant spectral shape features worth noting due to the assumed flat spectral shape of the Lambetian paint and the nearly spectrally flat shape of water reflection and transmission.

4.2.1 Effect of Water Contact Angle

Figure 8 shows BRDF plots in the specular scattering plane of incident angles of 20 and 60 degrees of a black painted surface with water drops covering 50% of the surface (calculated by area). The solid curve shows the painted surface in the absence of surface water and has a Lambertian (weighted by the cosine of the scattering angle for plotting purposes) shape as expected. The curve for the 180 degree contact angle drop has two distinct peaks, at a 20 degree angle of incidence, that are due to internal reflections arising from the same mechanism that causes rainbows in the sky. The rainbow peaks are not present for the 60 degree angle of incidence case due to shadowing effects resulting from the obilique viewing angle. The 15 degree contact angle water covered surface shows a broad peak centered about the 20 degree specular forward scattering angle, while the 90 degree contact angle curves approximately mimicking the dry surface for most scattering angles.

Also in Figure 8 are plots showing the ratio of the (1,0) to the (0,0) element of the pBRDF Mueller matrix. This ratio is analogous to a degree of S1 polarization calculation, but it maintains the sign of the (1,0) term. The degree of S1 polarization imparted by the water drops is most significant for the 180 degree contact angle case, which has significant peaks in both the forward and back scatter directions. The surface with the 15 degree contact angle water drops exhibits broad polarization peaks in the forward scatter direction around the specular reflection point, arising from the reflection from the top surface of the water drop.

4.2.2 Effect of Water Area Fraction

Finally, we kept the water contact angle constant at 90 degrees and varied the surface area coverage fraction of the water drops to examine its effect on BRDF magnitude and polarization. Water drop coverages of 5, 10, 30, 50, and 75% were simulated.

For an incident angle of 20 degrees, the pBRDF magnitude is essentially the same for all different area coverage values. This is likely due to the average Fresnel reflectance from the surface of water drop being approximately the same as the reflectance from the black painted surface. Due to the contact angle of 90 degrees, no significant reflection peak is observed because the first surface reflections are distributed across the entire hemisphere unlike small contact angle drops which have a more pronounced first surface reflection peak. For an incident angle of 60 degrees, as the water drop area coverage level increases we find more pronounced scattering in the oblique forward and back scattering directions which is likely due to rays entering the front of the water drop and leaving the backside without reflected from the black paint.

Finally, we find the degree of S1 polarization in the oblique forward scattering angles to increase as the water drop coverage level increases. The polarization of the light reflected into the oblique forward angles is due primarily to first surface reflections from the water drops.

5. SUMMARY

This paper has presented a new modeling capability to evaluate the spectral polarimetric reflectance properties of two different types of surface contamination cases. The first case examined the effect of soil particle concentration on changing the spectral appearance of a green painted surface. We found that increasing the soil particle surface coverage fraction transitioned the spectral shape of the surface signature at a rate that was not linear with this

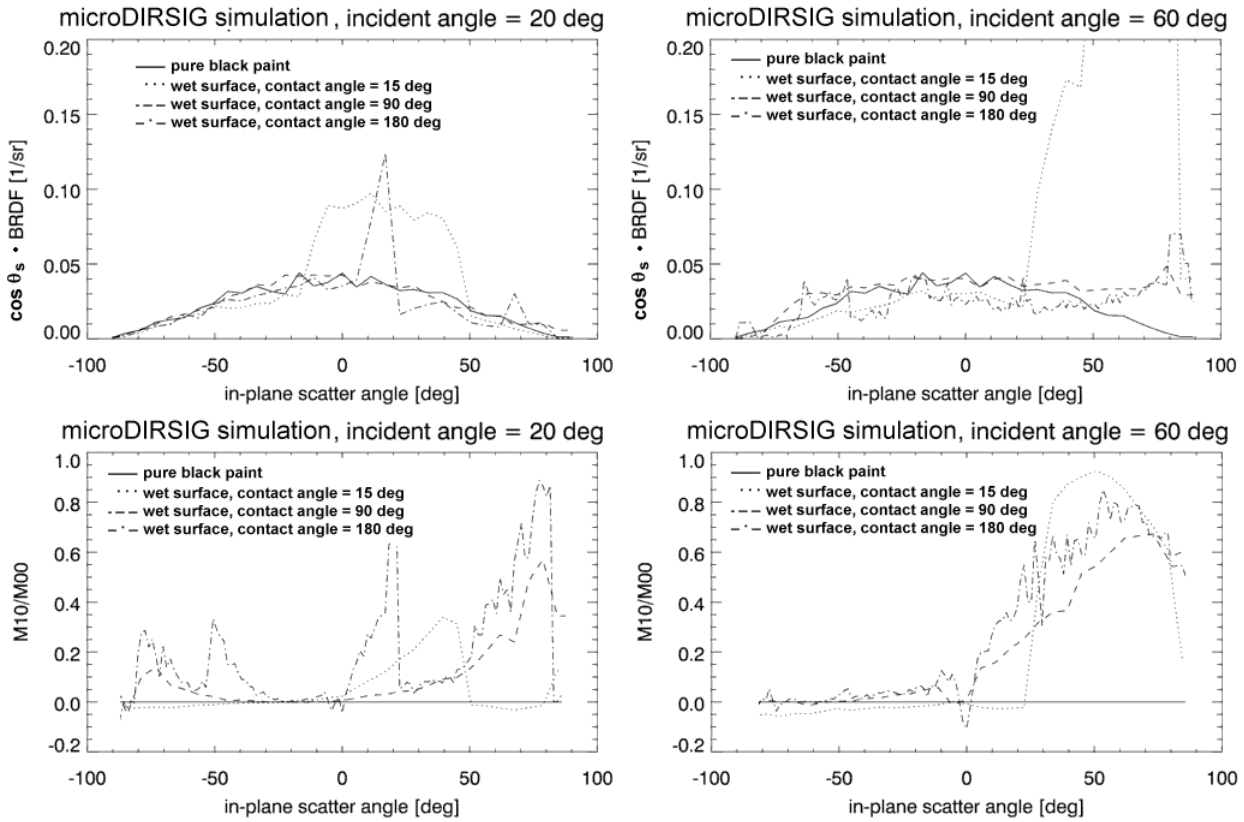

Figure 8. BRDF plots showing the unpolarized magnitude in the specular plane for incident angles of 20 and 60 degrees in the left and right columns respectively. The bottom row shows the ratio of the (1,0) to the (0,0) elements of the spectrally integrated pBRDF Mueller matrix, which is analogous to a degree of S1 polarization calculation which maintains the S1 sign. Each plot contains a curve for the clean black painted surface, and 50% water covered surface with contact angles of 15, 90, and 180 degrees.

fraction. This non-linear relationship was also found to be dependent on the angle of incidence of the source illumination. In addition, the spectral shape of the resulting contaminated surface cannot be found by a weighted sum of the soil and paint spectra due to the complex nature of the interactions between surface constituents and their different native BRDF shape. The de-polarization effect of the soil particles was also non-linear with respect to soil particle fraction.

The second surface contamination case examined the effects of surface water contact angle and area coverage fraction on polarized reflectance properties. The spectral shape of the contaminated surface in this case was flat in most cases due to the assumptions of the underlying surface spectral shape and the slowly varying spectral shape of water reflectance and transmission. However, we found significant polarization signatures were induced by the water drops with peak locations heavily dependent on the water contact angle. Similar to the soil contaminated surface case, we found the polarization of the surface by water drops to be non-linear in water drop area fraction.

Future work will examine a more realistic spatial distribution of contaminants across the modeled surfaces. In addition, we also plan to more finely sample the interesting phenomena observed for water contamination on a Lambertian surface. The water contact angles explored in this preliminary work (15, 90 and 180 degrees) are a very coarse sampling of this trade space and do not adequately examine the balance of first surface reflected, internally reflected, and transmission spectral polarimetric scattering phenomena.

6. ACKNOWLEDGMENTS

The authors wish to thank the Intelligence Community Post-Doctoral Fellowship Research program and Lockheed Martin Information Systems & Global Services Enterprise Integration Group for supporting this research.

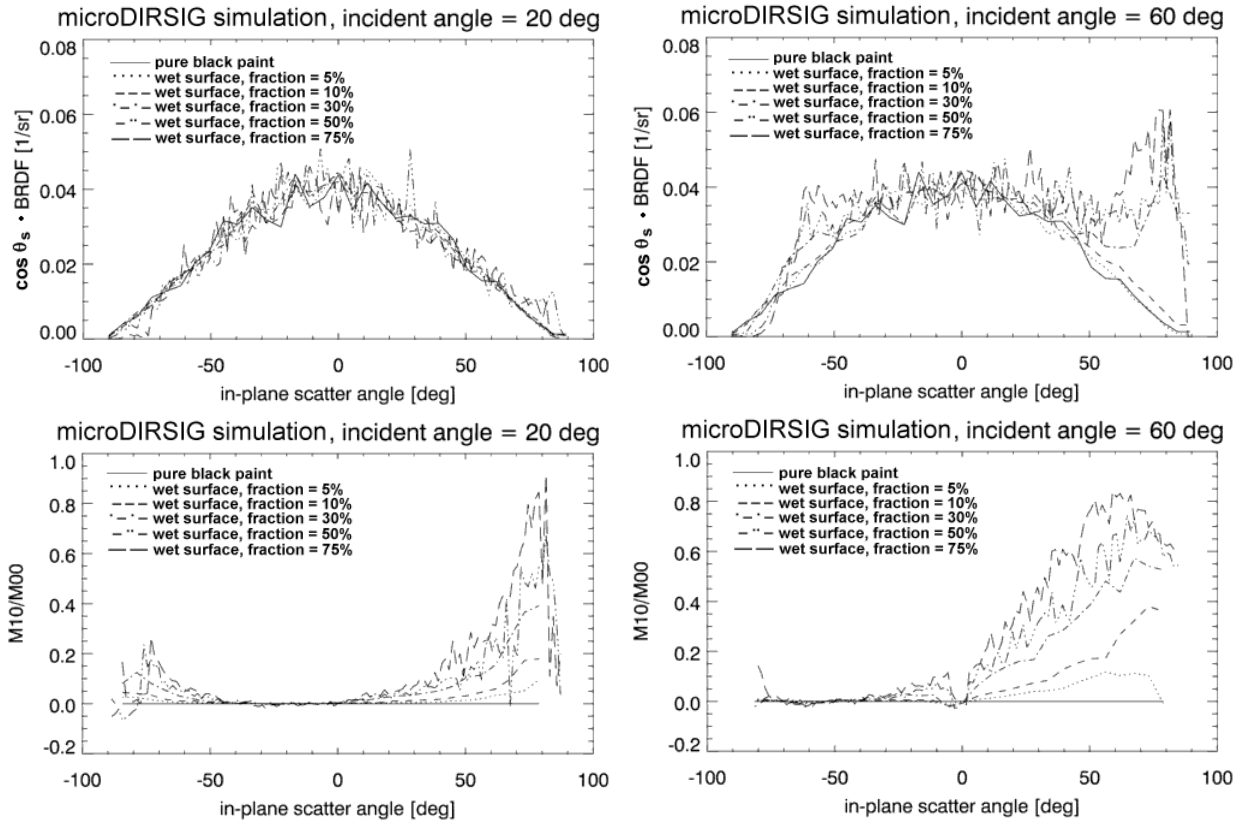

Figure 9. BRDF plots showing the unpolarized magnitude in the specular plane for incident angles of 20 and 60 degrees in the left and right columns respectively. The bottom row shows the ratio of the (1,0) to the (0,0) elements of the spectrally integrated pBRDF Mueller matrix, which is analogous to a degree of S1 polarization calculation which maintains the S1 sign. Each plots contains a curve for the clean black painted surface and a curve for 5, 10, 30, 50 and 75% water drop covered surfaces having a contact angle of 90 degrees.

REFERENCES

[1] Torrance, K. and Sparrow, E., "Theory for off-specular reflection from roughned surfaces," *Journal of Optical Society of America* **57**(9) (1967).

[2] Maxwell, J., Beard, J., Weiner, S., Ladd, D., and Ladd, S., "Bidirectional reflectance model validation and utilization," (1973).

[3] Priest, R. G. and Meier, S. R., "Polarimetric microfacet scattering theory with applications to absorptive and reflective surfaces," *Optical Engineering* **41**(5), 988–993 (2002).

[4] Phong, B. T., "Illumination for computer generated pictures," *Graphics and Image Processing* **18**, 311–317 (June 1975).

[5] Cook, R. L. and Torrance, K. E., "A reflectance model for computer graphics," in [*SIGGRAPH '81: Proceedings of the 8th annual conference on Computer graphics and interactive techniques*], 307–316, ACM, New York, NY, USA (1981).

[6] Ward, G., "Measuring and modeling anisotropic reflection," *Computer Graphics (Proceedings of SIGGRAPH 92* **26**, 265–272 (1992).

[7] [*Nonconventional Exploitation Factors Data System (NEFDS) Modeling Document v10*], National Geospatial Intelligence Agency (2006).

[8] Gartley, M., Brown, S., and Schott, J., "Micro-scale surface and contaminate modeling for polarimetric signature prediction," *Proc. of SPIE, Polarization: Measurement, Analysis, and Remote Sensing VIII* **6972** (2008).